PLEASE CITE THIS ARTICLE AS DOI: 10.1063/5.0083361

Transient Analysis of Photomultiplication-Type Organic Photodiodes

Songxue Bai[1], Ruiming Li[1], Huihuang Huang[1], Yiming Qi[1], Yalun Xu[1], Jiannan Song[1], Fang Yao[1], Oskar J. Sandberg[2], Paul Meredith[2], Ardalan Armin[2] and Qianqian Lin[1,]*

[1]Key Lab of Artificial Micro- and Nano-Structures of Ministry of Education of China, School of Physics and Technology, Wuhan University, Wuhan 430072, P. R. China

[2]Sustainable Advanced Materials Programme (Sêr SAM), Department of Physics, Swansea University, Singleton Park, Swansea SA2 8PP, United Kingdom

Corresponding Authors:

*Email: q.lin@whu.edu.cn

KEYWORDS: organic photodetectors, photomultiplication, transients, charge transport, pulsed-light detection

PLEASE CITE THIS ARTICLE AS DOI: 10.1063/5.0083361

ABSTRACT

Photomultiplication-type organic photodetectors have emerged as a class of next generation solution-processed photodetectors with high gain. Despite this promising feature, the reported photodectors still suffer from relatively large dark currents at high bias voltages. To overcome this drawback, a mechanistic understanding of photomultiplication effect in organic photodiodes is required. In this work, we advanced the performance of photomultiplication-type organic photodetectors by tuning the active layer composition and the interfacial layers. The optimized devices exhibit small dark currents and flat dark current-voltage curves at reverse bias condition up to -10 V. The optimized photodetectors also reached an ultra-high responsivity of 23.6 A/W and specific detectivity of 1.04×10^{12} Jones at -10 V. More importantly, we investigated the photomultiplication process with multiple transient techniques, and revealed that the photoconductive gain effect is a slow process, which relies on the photo-Schottky effect enabled by charge carrier tunneling and the accumulation of holes. Furthermore, we also demonstrated prototypical pulsed-light detection based on the optimized devices, which showed great potential for real applications.

INTRODUCTION

Organic semiconductors have attracted tremendous attention in the past few years, thanks to their excellent flexibility, solution-processability, low-cost and chemical versatility.[1-6] In particular, organic optoelectronic devices have also demonstrated compelling device performance. For instance, organic light emitting diodes (OLEDs) possess larger angle of visibility, fast response, better color contrast and flexibility, which enable their commercialization with great success.[7-10] The power conversion efficiency of organic solar cells (OSCs) has reached 18.89%, which is on a par with the well-established silicon technology.[11] Organic photodetectors (OPDs) have also demonstrated great potential for next generation photodetection both in visible and near-infrared, thanks to their variable optical bandgaps, solution processability, light weight and mechanical flexibility.[12-17] More recently, photomultiplication-type (PM-type) OPDs have presented extremely high external quantum efficiency (EQE) and responsivity, which is very attractive for weak light detection without pre-amplification and could potentially overcome the conventional charge transport limited low detectivity of OPDs.[18-23] In 2008, Chen and co-workers combined CdTe nanoparticles with OPDs and realized high photoconductive gain based on the diode structure.[24] Later on, Guo *et al.* reported multiplication-type OPDs based on interfacial trap-controlled charge injection, and achieved ultraviolet photodetectors with ultrahigh responsivity.[25] Li *et al*. reported a relatively high EQE of 16700% at -19 V based on small amount of [6,6]-phenyl C71-butyric acid methyl ester ($PC_{71}BM$) doped Poly (3-hexylthiophene-2,5-diyl) (P3HT) (~1wt%), and attributed this PM

effect to the accumulation of electrons near the metal electrode which causes band bending at the interface, resulting in a large photocurrent generated as holes are injected by tunneling.[26] Shen and co-authors further extended the sensitivity of the PM-type OPDs to near-infrared region.[27] Wang and co-authors also reported PM-type OPDs based on non-fullerene acceptors, and fabricated excellent broadband photodetectors.[28] Furthermore, Wang *et al.* and Kublitski *et al.* achieved narrowband PM-type OPDs for near-infrared photodetection, based on the sub-bandgap absorption, respectively.[29, 30] Liu *et al*. also reported ternary blend based PM-type OPDs, which exhibited a narrow response with FWHM of 27 nm and a high EQE up to 29700% at -13 V.[31]

Despite the great success of enhanced device performance and extended detection bandwidth of PM-type OPDs, most of the reported PM-type OPDs exhibit relatively high dark current and noise, since the devices normally require high bias voltage to trigger the PM-effect. However, the PM-type OPDs normally display large leakage current and poor stability under high electrical field, which limit the real applications of the PM-type OPDs to some extent. Secondly, the underlying mechanism of photomultiplication effect is generally attributed to the trap-mediated charge transport, and lacks of detail analysis. There is no clear physical model to fully characterize the photomultiplication process, in particular for short time-scales. In addition, the reported PM-type OPDs are mainly focused on the tunability of spectral response and gain factor. The application of PM-type devices in other field has barely been reported, and requires more research activities. To fill these gaps, we fabricated PM-type OPDs

based on ternary blends, composed of 4,4'-cyclohexylidenebis[*N*,*N*-bis(*p*-tolyl)aniline] (TAPC) and poly(3-hexylthiophene-2,5-diyl) (P3HT) as donor materials and [6,6]-phenyl-C61-butyric acid methyl ester ($PC_{61}BM$) as acceptor. We try to optimize the weight radios of the blends, the interfacial layers and the thickness to suppress the dark current and device leakage at high reverse bias voltage. More importantly, we introduce multiple transient techniques to record the PM process and investigate the devices in detail, including transient photocurrent, double injection, transient photovoltage, transient capacitance and dielectric response in frequency domain. We further introduce the PM-type OPDs to detect the pulsed weak light, benefiting from the observed slow-response feature of the PM process.

RESULTS AND DISCUSSION

Prior to the transient characterizations, we first optimized the device structure and investigated their performance metrics. **Figure 1a** schematically depicts the device architecture of the PM-type OPDs used in this work. We incorporated a wide bandgap donor TAPC into P3HT matrix, which could effectively reduce the conductivity of the active layer and did not change the absorption spectra as shown in **Figure S1**. **Figure 1b** displays the energy level diagram of the device, indicating that the photogenerated carriers can be easily transferred within the ternary blends due to the offset of highest occupied molecular orbital (HOMO) and lowest unoccupied molecular orbital (LUMO) levels, that is, the generated electrons are transferred from donors to $PC_{61}BM$ and the holes are extracted by the donors. In addition, the relatively high

HOMO of TAPC can effectively block the transport of electron, which is beneficial for suppressing the dark current. However, with excessive amount of TAPC, the charge generation decreases significantly due to the diluted absorber. **Figure S2a** compares the *J-V* curves of the OPDs with thin active layers (~260 nm) and various blending ratios in dark and under illumination. With the increased amount of TAPC, the gain effect increased at high reverse bias conditions. However, these OPDs still possess relatively high dark current. We further increased the active layer thickness up to ~550 nm. The device performance shown in **Figure S2b** indicates that the dark current reduced significantly and PM effect was also enhanced. We chose the optimal composition of TAPC:P3HT:$PC_{61}BM$ to be 10:40:1, and further optimized the interlayers, including the thickness of electron transport layer ZnO and the concentration of PEIE, as shown in **Figure S2c** and **2d**, respectively. The optimized devices based on 35 nm ZnO and 0.2wt% PEIE showed ultra-low and bias-independent dark current of ~ 10 nA/cm^2. **Figure 1c** displays the light intensity dependent *J-V* curves. With the increase of light intensity, the PM-effect was enhanced remarkably at high reverse bias voltage. **Figure 1d** shows the typical bias-dependent EQE spectra of the optimized PM-type OPDs under 0.3 mW/cm^2 illumination, indicating relatively high gain effect at bias conditions, which is consistent with the measured *J-V* curves. **Figure S3** presents the typical noise spectra of the optimized PM-type OPDs at various reverse bias voltages, and **Figure 1e** compares the bias-dependent noise, including calculated Johnson (thermal) noise, shot noise and measured total noise, which increased slightly with the increase of bias

voltage given by (assuming bandwidth of 1 Hz), [32]

$$i_{\text{total}} = \sqrt{i_{\text{shot}}^2 + i_{\text{johnson}}^2 + i_{1/f}^2} = \sqrt{2eJ_{\text{d}} + \frac{4k_{\text{b}}T}{R_{\text{sh}}} + i_{1/f}^2} \qquad (1)$$

where J_{d} is the dark current, k_{b} is Boltzmann constant, T is temperature and R_{sh} is the shunt resistance obtained from the recorded *J-V* curves, while $i_{1/f}^2$ represents the Flicker noise. It is worth to note that the measured noise exhibited stronger bias dependence and larger magnitude than the calculated shot and thermal noise at relatively low frequency. It could be attributed to the increased Flicker noise and device leakage caused by the high electric field. Having the knowledge of EQE and noise, we can further calculate the noise equivalent power (NEP) and specific detectivity (D^*) as follows, [33, 34]

$$\text{NEP} = \frac{i_{\text{total}}}{R} = \frac{h \cdot c \cdot i_{\text{total}}}{\text{EQE} \cdot e \cdot \lambda} \qquad (2)$$

$$D^* = \frac{R\sqrt{AB}}{i_{\text{total}}} = \frac{\text{EQE} \cdot e \cdot \lambda \cdot \sqrt{A \cdot B}}{h \cdot c \cdot i_{\text{total}}} \qquad (3)$$

where R is responsivity, A is the device area, B is the testing bandwidth, i_{total} is the measured noise current, c is the speed of light, e is the elementary charge, h is Plank constant and λ is the wavelength. **Figure S4** displays the typical NEP spectra of the optimized Pm-type OPDs at various bias voltages. **Figure 1f** displays the bias dependent specific detectivity of the optimized PM-type OPDs calculated based on the measured noise and inferred from the shot noise. Detectivity is a balance of EQE and noise, and the highest D^* reached ~10^{12} Jones at -10 V, which is comparable with the reported PM-type OPD, summarized as shown in **Table S1**.

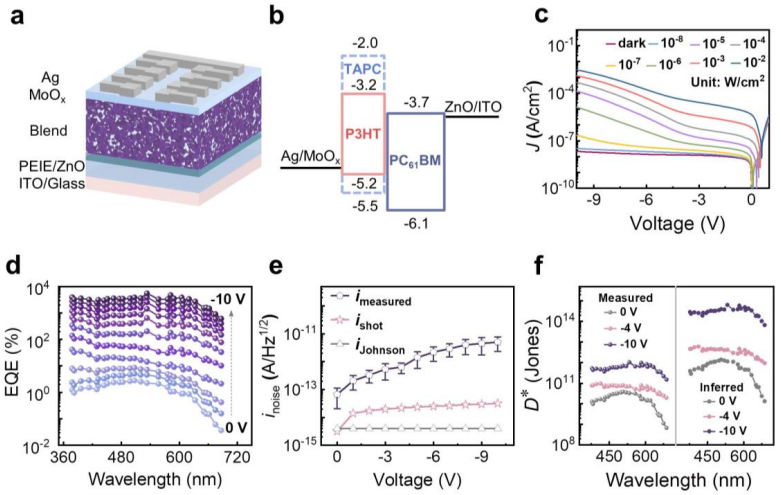

Figure 1. Schematic illustration of the (**a**) device structure and (**b**) energy levels of the PM-type OPDs based on $PC_{61}BM$ doped P3HT. (**c**) Comparison of the *J-V* curves obtained in dark and under various light intensities from 10^{-8} to 10^{-2} W/cm^2, indicating a remarkable PM-effect under large reverse bias voltages. (**d**) The bias voltage dependent EQE spectra of the devices from 0 V to -10 V, the EQE increased more than three orders of magnitude. (**e**) Noise spectra and (**f**) specific detectivity of the optimized PM-type OPDs tested at various reverse bias voltages, suggesting a strongly bias-dependent performance.

Having obtained well-performed PM-type OPDs, we now turn to the analysis of the underlying working mechanism of the PM process. Most of the reported work claimed that it should be related with the trap states and interfacial energetic barriers. Hence, we first evaluated temperature-dependent performance metrics of the OPDs as shown in **Figure 2a**. **Figure S5** further presents the light intensity dependent *J-V* curves at various temperatures. Intriguingly, all the PM-type OPDs did not show

PLEASE CITE THIS ARTICLE AS DOI: 10.1063/5.0083361

critical influence on the dark and light *J-V* curves. We also compared the light intensity dependent photocurrent at -2 V and -10 V as a function of temperature in **Figure 2b** and **2c**. Then we determined the activation energy to be 10.23 and 5.2 meV based on the Arrhenius law, indicating negligible temperature dependency and the total current at these voltages is not limited by the thermally-activated processes. Furthermore, we also tested the charge carrier dynamics of the active layers with and without doping of $PC_{61}BM$ via time-resolved microwave conductivity (TRMC, see more details in **supplementary Note 1**) as shown in **Figure 2d**. Compared with the pristine P3HT films, the conductivity of the 2% $PC_{61}BM$ doped films showed improved charge carrier mobility from ~3×10^{-4} $cm^2/(V\cdot s)$ to 1.6×10^{-3} $cm^2/(V\cdot s)$. Moreover, a prolonged carrier lifetime of ~ 20 μs was observed from the TMRC decay, indicating the build-up of carrier concentration within the active layers under the illumination of pulsed excitation.[35-37] To verify the improved charge carrier mobility, we also performed load-resistance dependent photovoltage (RPV) measurements on operational devices.[38] Similarly, the 2% $PC_{61}BM$ doped P3HT based devices showed much faster transit time, resulting more than an order of magnitude higher mobility, which is consistent with TRMC results.

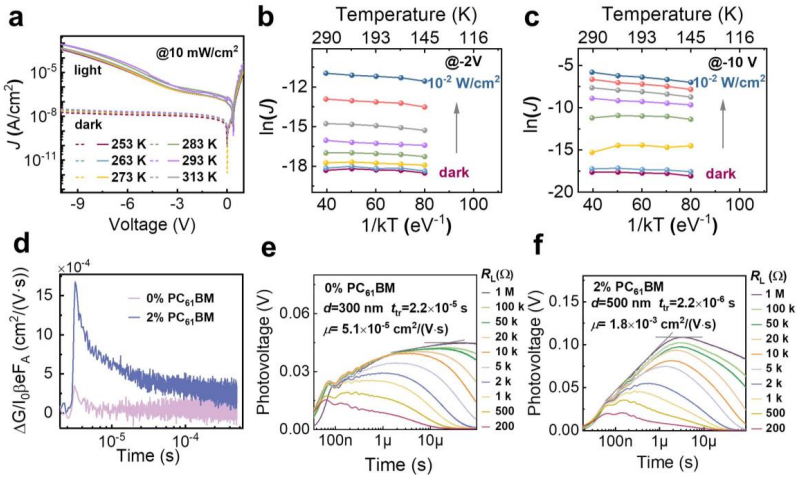

Figure 2. (**a**) Temperature dependent *J-V* curves of the optimized PM-type OPDs in dark and under 10 mW/cm^2 illumination, temperature dependent dark and photocurrent of the PM-type OPDs measured at (**b**) -2 V and (**c**) -10 V, (**d**) mobility of pristine P3HT and P3HT doped with 2% $PC_{61}BM$, measured with time-resolved microwave conductivity, load-resistance dependent photovoltage transients of (**e**) the pristine P3HT films and (**f**) 2% $PC_{61}BM$ doped P3HT films. .

To figure out the underlying mechanism of the photomultiplication effect, we further performed transient photocurrent measurements as shown in **Figure 3**. To decouple the influence of illumination and voltage bias on the current transients, we performed the biasing separately. **Figure 3a** schematically illustrates the testing conditions of the devices under modulated light source and constant voltage bias, and the recorded voltage dependent photocurrent transients are displayed in **Figure 3b**. **Figure 3c** further compared the current transients as a function of time, and we found the devices presented relatively fast temporal response at low bias conditions. With

further increase of the reverse bias, the photocurrent increased significantly, *i.e.*, photoconductive gain. However, this process is much slower compared with the charge transport process, which is normally in the time-scale of microseconds. Then, we further collected the bias voltage dependent photocurrent at various time-scales as shown in **Figure 3d**. Intriguingly, the reconstructed transient *J-V* curves exhibited increased gain effect under high bias voltage and in a long time-scale, and the transient *J-V* collected at 1 ms was approaching the steady-state *J-V* curve measured with source meter, indicating the saturation of the photocurrent requires around 1 ms. For comparison, we also tested the devices under continuous light bias and modulated the bias voltage as depicted in **Figure 3e**. The recorded current transients both in dark and under illumination are shown in **Figure 3f**. We can also reconstruct the transient *J-V* curves as shown in **Figure 3g**, which showed similar trend as we shown in **Figure 3d**. **Figure S6** further compares the temporal photoresponse under various bias conditions with multiple cycles, and we can observe that the response speed was slowed down under large reverse bias conditions. Furthermore, we also fabricated OPD devices based on pristine P3HT films and conventional P3HT:$PC_{61}BM$ (1:1) bulk-heterojunctions (BHJs), and tested their transient photocurrent as shown in **Figure S7**. We did not observe such slowly increasing photoconductive gain from the control devices.

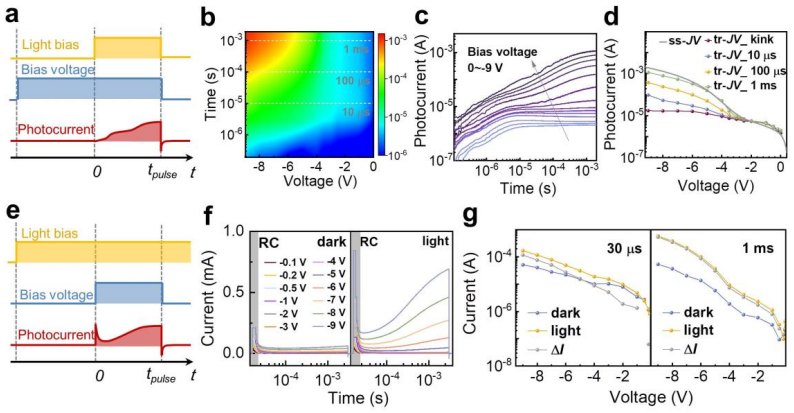

Figure 3. (**a**) Schematic illustration of transient current measured with pulsed light and constant bias voltages, (**b**) the contour plot of the photocurrent as a function of bias voltage and time, (**c**) selected photocurrent transients at various bias voltages, (**d**) comparison of the reconstructed transient *J-V* curves and the recorded steady-state *J-V* curve, (**e**) schematic illustration of transient current measured with pulsed bias voltage and constant illumination, and (**f**) the comparison of the recorded current transients measured in dark and under illumination, (**g**) the reconstructed transient *J-V* curves at 30 μs and 1 ms.

We further compared their dielectric response in dark and under illumination in frequency domain (**Figure 4a-d**), and found the 2% doped devices showed relatively large real part of the dielectric constant, indicating considerable photo-induced polarization. For the 2% $PC_{61}BM$ doped samples, we also observed dielectric loss peaks from the imaginary part of the dielectric constants, reflecting that such polarization induced PM-process mainly appears around 10 kHz, corresponding to 100 μs, which is consistent with the photocurrent transients. In addition, we also

performed the transient photovoltage measurements of these OPDs with various concentrations of $PC_{61}BM$ as shown in **Figure 4e-h**. The conventional BHJ exhibited a fast rise time, indicating excellent charge extraction and accumulation on the electrodes.[39] The pristine P3HT films demonstrated relatively small photovoltage due to the unipolar charge transport and poor charge accumulation on both electrodes. On the contrary, the 2% $PC_{61}BM$ doped OPDs showed a slowly increasing photovoltage, indicating that the charge transport within the doped P3HT films is efficient but unbalanced, and the unbalance charge transport may easily result the accumulation of charge carrier density and photoconductive gain. Overall, these evidences collectively showed that the PM process is relatively slow and should be correlated with the light induced polarization and unbalanced charge transport induced charge accumulation. Hence, the PM process can be enhanced with the increase of light intensity, bias voltage and accumulation time.

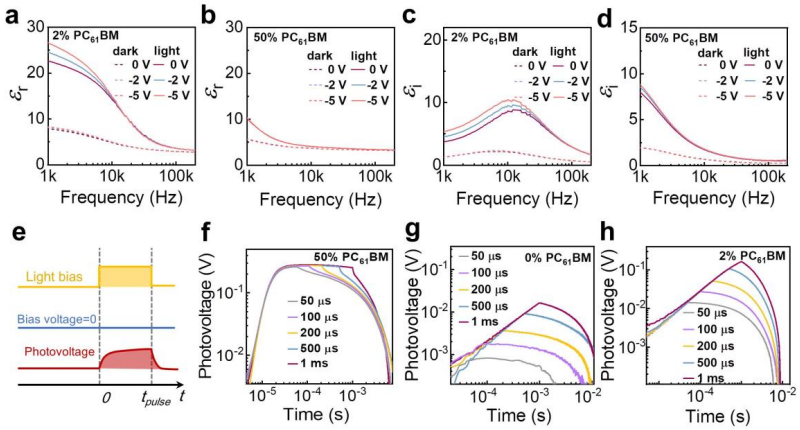

Figure 4. Real part of the dielectric constants measured in dark and under illumination of the P3HT films blended with (**a**) 2% and (**b**) 50% $PC_{61}BM$, imaginary

part of the dielectric constants measured in dark and under illumination of the P3HT films blended with (**c**) 2% and (**d**) 50% $PC_{61}BM$. (**e**) Schematic illustration of the transient photovoltage measurement with various pulse lengths of the light source, recorded transient photovoltage of the devices based on P3HT with (**f**) 50% $PC_{61}BM$, (**g**) 0% and (**h**) 2% $PC_{61}BM$.

To fully understand the charge injection process of the PM-type devices, we performed capacitance-voltage (CV) and transient capacitance measurements. Based on the light intensity dependent CV profiling (as shown in **Figure S8**), we can determine the effective doping level of the active layers. Intriguingly, the 2% doped PM-type devices exhibited significant change under illumination. Based on the voltage dependent $1/C^2$ curves, we can obtain the effective doping level (N_{dop}),

$$N_{\mathrm{dop}} = \frac{2(V_{\mathrm{bi}} - V_{RB})}{e\varepsilon\varepsilon_0 A^2 C^{-2}} \qquad (4)$$

where V_{bi} is the build-in field, V is bias voltage, C is the device capacitance, ε is the dielectric constant, ε_0 is the vacuum permittivity, e is the elementary charge and A is the device area.[40] The reduced slope of the $1/C^2$ curves suggested an increased effective doping density. Furthermore, we also recorded the transient capacitance at various reverse bias voltages (V_{RB}), and the devices were perturbed with a bias pulse (V_{pulse}) as depicted in **Figure 5a**. Transient capacitance also known as deep-level transient spectroscopy (DLTS), is a powerful technique, which can effectively probe the trap density, capture cross-section and trap emission rates *etc.*, by filling charge carriers to the trap states within the space charge region at forward bias and extracting

the trapped carriers at reverse bias.[41] This technique can also distinguish the carrier type, *i.e.,* positive transient capacitance (ΔC_{max_p}) implies minority carriers injection and negative transient capacitance (ΔC_{max_n}) suggests majority carriers injection, for p-type semiconductors.[41] **Figure S9** schematically illustrated the typical capture and emission processes of the minority and majority carriers of a typical p-type semiconductor. The capture and thermal emission rates of electrons are C_e and E_e, and the capture and thermal emission rates of holes in this case are C_h and E_h, respectively. In the quiescent state, the traps within depletion region are observable by tuning the reverse bias voltage. Within a pulsed charge injection at forward bias, the traps could be filled, which modulated the device capacitance simultaneously. However, the capacitance will return to its quiescent value after all the carriers are emitted back to the initial states. The sign of the capacitance change depends on whether the electron occupation of the trap states has been increased or decreased by the pulse.[41] **Figure 5b** displays the typical transient capacitance decays of the optimized 2% doped devices under the illumination of 170 μW/cm^2. A large amount of the minority traps were filled after the pulse voltage at relatively low reverse bias voltage. However, another negative ΔC decay were observed at relatively high reverse bias voltage, indicating the injection of significant amount of the majority carriers (holes). Then, we further increased the light intensity to ~2 mW/cm^2, as shown in **Figure 5c**. The minority injection was inhibited, but the hole injection was significantly enhanced. For comparison, we also recorded the transient capacitance of the pristine P3HT films and the 50% $PC_{61}BM$ doped P3HT films as shown in **Figure 5d** and **5e**. We observed

a negligible negative capacitance change from the 50% samples, and a small positive capacitance change from the pristine P3HT films, indicating less charge injection and trap concentration for both devices. In addition, we did not observe the transition between minority and majority carrier as we observed from the 2% devices. We also extracted the C_{max} of both carriers of the 2% $PC_{61}BM$ doped P3HT devices, and plotted as a function of bias voltage as shown in **Figure 5f**. Interestingly, the transition appeared at much lower reverse bias voltage of ~ 4 V, which is close to the onset of the PM process obtained from *J-V* curves as shown in **Figure 1c**. We also revealed the emission rates or lifetimes of the trapped carriers as shown in **Figure S10**. The injected holes have much smaller emission rate than the electrons, *i.e*., longer lifetime, leading to the effective build-up of carriers within the space charge region. Again, these results are consistent with the observed trend as we discussed previously, that is, the PM-process can be enhanced with the increase of light intensity, reverse bias voltage and accumulation time.

We also compared their CV both in dark and under 2 mW/cm^2 illumination (**Figure S11**), and found the pristine P3HT and 50% doped P3HT films were light insensitive. However, the 2% samples showed remarkable change under illumination. Hence, the PM process should be light activated, which effectively increased the effective doping density as aforementioned. The increased doping density can result a space charge region near cathode with a large band-bending, as schematically depicted in **Figure 5g**. Then, the injected holes or the onset voltage of the hole injection can be correlated with effective doping density and tunneling distance (x_0) as shown in **Figure 5h**.

Conventionally, the tunneling distance of organic semiconductors are around 2~5 nm. Then, a high doping level of ~10^{18} cm^3 can easily result a very low onset voltage of ~4 V. We also compared the inferred doping density with the N_{dop} values obtained from the light intensity dependent CV, as shown in **Figure 5i**. Interestingly, the determined effective doping density under > 10 μW/cm^2 illumination is exactly located within the range of effective tunneling distance, validating photo-Schottky effect inducing charge tunneling.

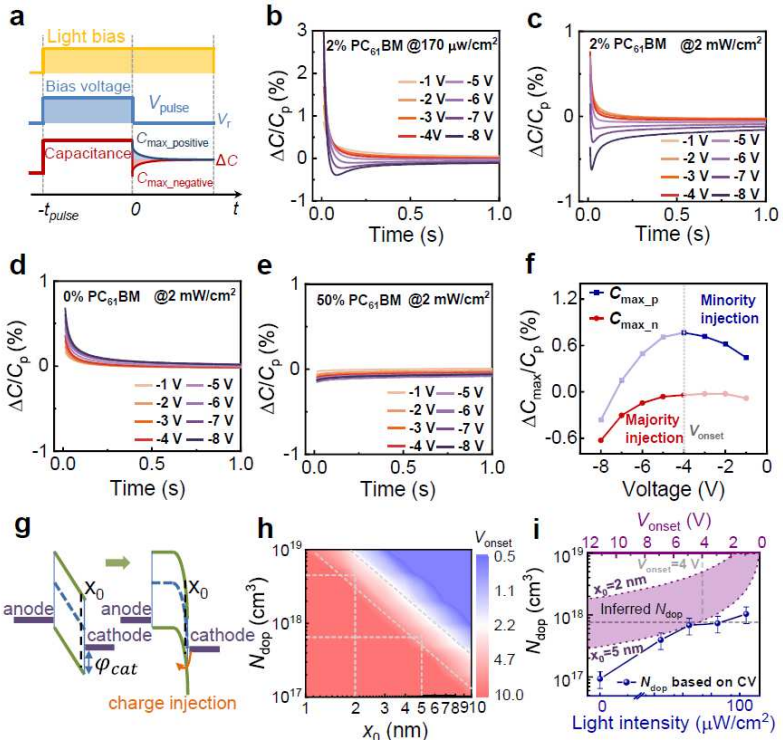

Figure 5. (**a**) Schematic illustration of the transient capacitance measurement, and the recorded transient capacitance decay of the 2% $PC_{61}BM$ doped P3HT devices under (**b**) 170 μW/cm^2 and (**c**) 2 mW/cm^2 illumination, (**d**) transient capacitance of the the

pristine P3HT and (e) 50% $PC_{61}BM$ doped P3HT devices, (**f**) extracted maximum transient capacitance of the 2% $PC_{61}BM$ doped P3HT devices caused by the injection of minority and majority carriers under 2 mW/cm^2, (**g**) schematic comparison of the charge injection of the 2% $PC_{61}BM$ doped devices in dark and under illumination, (**h**) contour plot of the PM onset voltage as a function of effective doping level and tunneling distance and (**i**) the comparison of the effective doping density inferred from the tunneling distance and the values obtained from CV.

Having established the basic operation principle of the PM-type OPDs, we now turn to the application of these devices. As the PM process requires much longer time, the photocurrent decay is also extremely slow. Hence, we could introduce this accumulation effect for weak pulsed light detection. Conventionally, the detection of pulsed-light is quite challenging, and requires ultra-fast photodetectors and recording systems, such as oscilloscope with large bandwidth. Alternatively, thermal detectors are also commonly used for pulse-light detection due to the accumulation effect. However, most of the detectors based on thermal effects are relatively slow and lacks of accuracy.[42] Hence, it is urgent to develop other technique to efficiently detect pulsed-light with facile equipment. Here, we tested the PM-type OPDs under pulsed light (10 kHz) as shown in **Figure 6a**. Interestingly, the photocurrent of the devices under large reverse bias conditions increased slowly under pulsed light sources. However, we did not observe such accumulation effect from the conventional BHJs and the 2% doped devices under low bias voltage conditions as shown in **Figure 6b**. We also tested the devices under various wavelengths, and found the same trend. The

inset of **Figure 6c-e** also exhibits a linear relationship between the light intensity and saturated photocurrent, indicating the feasibility of applying PM-type OPDs for pulsed-light detection in a wide range. Moreover, we can also replace the costly oscilloscope with a simple multimeter to record the light intensity of the pulse-light, as we demonstrated in **Figure S12**. In addition, the photocurrent of the PM-type OPDs is also highly dependent on the modulation frequency (as shown in **Figure S13**), since the devices are mainly working based on the accumulation process. The photocurrent increased almost linearly with the increase of frequency, and it also saturated much faster at high frequency. Hence, these devices are working more like an energy detector instead of conventional power detector. Based on the PM effect, we can easily achieve pulsed-light detection without recording the current transients, and also reduced the detection cost and limit.

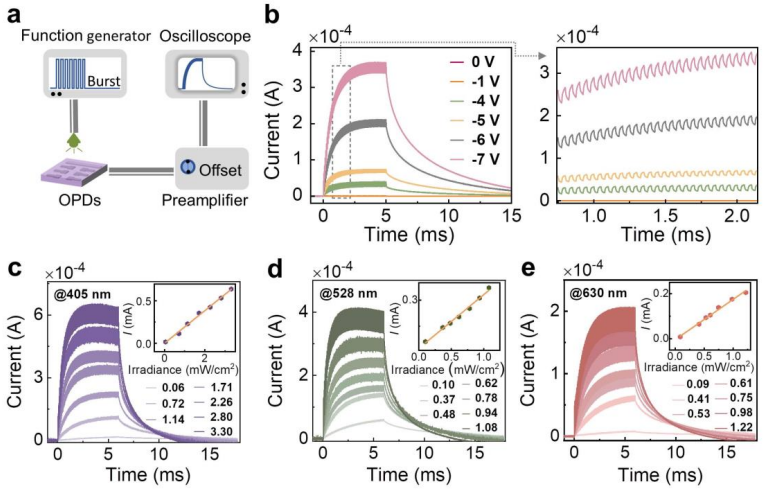

Figure 6. (**a**) Schematic illustration of the pulsed-light detection system, (**b**) recorded photocurrent transient of the PM-type OPDs under 10 kHz modulated light at various

reverse bias conditions (from 0 V to-7 V), photocurrent transients of the optimized PM-type OPDs at -6 V under (**c**) 405 nm light sources with various light intensities from 0.06 to 3.3 mW/cm^{-2}, (**d**) 528 nm light sources with various light intensities from 0.1 to 1.08 mW/cm^{-2} and (**e**) 630 nm light sources with various light intensities from 0.09 to 1.22 mW/cm^{-2}. The insets present the light intensity dependent photocurrent retrieved from the photocurrent transients shown in (**c**-**e**), respectively.

CONCLUSION

In summary, we first optimized PM-type OPDs by tuning the active layer composition, interlayer thickness and interfacial modification, and achieved relatively low dark current and high responsivity. Then, we analyzed the optimized PM-type OPDs with multiple transient techniques and found the PM effect was a slow process. The PM process is also correlated with the charge injection by photo-Schottky effect induced tunneling and charge accumulation. These results collectively prove the slow feature of the photoconductive gain, and we further introduced this effect for weak pulsed light detection. Prototypical devices were tested both with oscilloscope and multimeter, which demonstrated excellent response to the pulsed-light benefiting from the PM effect. These results further indicate the great potential of PM-type OPDs for next-generation photodetection and real applications.

ACKNOWLEDGEMENTS

This work was financially supported by the National Natural Science Foundation of China (Grant No. 61875154), Natural Science Foundation of Jiangsu Province, China

(Grant No. BK20190214), the National Key R&D Program of China (Grant No. 2020YFB2008800), and Project funded by China Postdoctoral Science Foundation (2021M702513).

SUPPLEMENTARY MATERIAL

See the supplementary material for the experimental details, supporting notes on analysis of TRMC data and calculation of hole injection induced by tunneling, and supporting figures S1-S13.

DATA AVAILABILITY

The data that support the findings of this study are available from the corresponding authors upon reasonable request.

REFERENCES

[1]H. Dong, H. Zhu, Q. Meng, X. Gong and W. Hu, ***Chem. Soc. Rev.*** **41** (5), 1754 (2012).
[2]C. Liu, K. Wang, X. Gong and A. J. Heeger, ***Chem. Soc. Rev.*** **45** (17), 4825 (2016).
[3]Z. Zhao, C. Xu, L. Niu, X. Zhang and F. Zhang, ***Laser Photon. Rev.*** **14** (11), 2000262 (2020).
[4]P. C. Y. Chow and T. Someya, ***Adv. Mater.*** **32** (15), 1902045 (2020).
[5]H. Huang, L. Jiang, J. Peng, Y. Qi, S. Bai and Q. Lin, ***Chem. Mat.*** **33** (20), 8089 (2021).
[6]A. Armin, M. Hambsch, I. K. Kim, P. L. Burn, P. Meredith and E. B. Namdas, ***Laser Photon. Rev.*** **8** (6), 924 (2014).
[7]C.-Y. Chan, M. Tanaka, Y.-T. Lee, Y.-W. Wong, H. Nakanotani, T. Hatakeyama and C. Adachi, ***Nat. Photonics*** **15** (3), 203 (2021).
[8]J. Song, H. Lee, E. G. Jeong, K. C. Choi and S. Yoo, ***Adv. Mater.*** **32** (35), 1907539 (2020).
[9]S. Choi, C.-M. Kang, C.-W. Byun, H. Cho, B.-H. Kwon, J.-H. Han, J.-H. Yang, J.-W. Shin, C.-S. Hwang, N. S. Cho, K. M. Lee, H.-O. Kim, E. Kim, S. Yoo and H. Lee, ***Nat. Commun.*** **11** (1), 2732 (2020).
[10]Y.-H. Kim, T.-H. Han, C. Lee, Y.-H. Kim, Y. Yang and T.-W. Lee, ***Adv. Funct. Mater.*** **30** (46), 2005292 (2020).
[11]S. Bao, H. Yang, H. Fan, J. Zhang, Z. Wei, C. Cui and Y. Li, ***Adv. Mater.*** **33** (48), 2105301 (2021).
[12]Y. Xu and Q. Lin, ***Appl. Phys. Rev.*** **7** (1), 011315 (2020).

[13]J. Kublitski, A. Hofacker, B. K. Boroujeni, J. Benduhn, V. C. Nikolis, C. Kaiser, D. Spoltore, H. Kleemann, A. Fischer, F. Ellinger, K. Vandewal and K. Leo, ***Nat. Commun.*** **12** (1), 551 (2021).
[14]J. Liu, Y. Wang, H. Wen, Q. Bao, L. Shen and L. Ding, ***Sol. RRL*** **4** (7), 2000139 (2020).
[15]Z. Lan, Y. Lei, W. K. E. Chan, S. Chen, D. Luo and F. Zhu, ***Sci. Adv.*** **6** (5), eaaw8065 (2020).
[16]Z. Lan, Y. S. Lau, Y. Wang, Z. Xiao, L. Ding, D. Luo and F. Zhu, ***Adv. Opt. Mater.*** **8** (24), 2001388 (2020).
[17]K. Yang, Z. Zhao, M. Liu, Z. Zhou, K. Wang, X. Ma, J. Wang, Z. He and F. Zhang, ***Chem. Eng. J.*** **427**, 131802 (2022).
[18]Z. Zhao, J. Wang, C. Xu, K. Yang, F. Zhao, K. Wang, X. Zhang and F. Zhang, ***J. Phys. Chem. Lett.*** **11** (2), 366 (2020).
[19]Z. Zhao, M. Liu, K. Yang, C. Xu, Y. Guan, X. Ma, J. Wang and F. Zhang, ***Adv. Funct. Mater.*** **31** (43), 2106009 (2021).
[20]Z. Zhao, C. Li, L. Shen, X. Zhang and F. Zhang, ***Nanoscale*** **12** (2), 1091 (2020).
[21]S. G. Han, H. Lee, W. Choi, D. Lee, S. Kim, Y. Sung, S. Kim and K. Cho, ***Adv. Funct. Mater.*** **31** (31), 2102087 (2021).
[22]M. Liu, J. Wang, K. Yang, Z. Zhao, Z. Zhou, Y. Ma, L. Shen, X. Ma and F. Zhang, ***J. Mater. Chem. C*** **9** (19), 6357 (2021).
[23]S. Xing, J. Kublitski, C. Hänisch, L. C. Winkler, T.-Y. Li, H. Kleemann, J. Benduhn and K. Leo, ***Adv. Sci.***, 2105113 (2022).
[24]H.-Y. Chen, M. K. F. Lo, G. Yang, H. G. Monbouquette and Y. Yang, ***Nat. Nanotechnol.*** **3** (9), 543 (2008).
[25]F. Guo, B. Yang, Y. Yuan, Z. Xiao, Q. Dong, Y. Bi and J. Huang, ***Nat. Nanotechnol.*** **7** (12), 798 (2012).
[26]L. Li, F. Zhang, J. Wang, Q. An, Q. Sun, W. Wang, J. Zhang and F. Teng, ***Sci. Rep.*** **5** (1), 9181 (2015).
[27]L. Shen, Y. Fang, Q. Dong, Z. Xiao and J. Huang, ***Appl. Phys. Lett.*** **106** (2), 023301 (2015).
[28]W. Wang, F. Zhang, H. Bai, L. Li, M. Gao, M. Zhang and X. Zhan, ***Nanoscale*** **8** (10), 5578 (2016).
[29]W. Wang, F. Zhang, M. Du, L. Li, M. Zhang, K. Wang, Y. Wang, B. Hu, Y. Fang and J. Huang, ***Nano Lett.*** **17** (3), 1995 (2017).
[30]J. Kublitski, A. Fischer, S. Xing, L. Baisinger, E. Bittrich, D. Spoltore, J. Benduhn, K. Vandewal and K. Leo, ***Nat. Commun.*** **12** (1), 4259 (2021).
[31]M. Liu, J. Wang, Z. Zhao, K. Yang, P. Durand, F. Ceugniet, G. Ulrich, L. Niu, Y. Ma, N. Leclerc, X. Ma, L. Shen and F. Zhang, ***J. Phys. Chem. Lett.*** **12** (11), 2937 (2021).
[32]J. Wang, S. Ullbrich, J.-L. Hou, D. Spoltore, Q. Wang, Z. Ma, Z. Tang and K. Vandewal, ***ACS Photonics*** **6** (6), 1393 (2019).
[33]Q. Lin, A. Armin, P. L. Burn and P. Meredith, ***Nat. Photonics*** **9** (10), 687 (2015).
[34]Y. Fang, A. Armin, P. Meredith and J. Huang, ***Nat. Photonics*** **13** (1), 1 (2019).
[35]Y. Liu, Y. Gao, B. Xu, P. H. M. Van Loosdrecht and W. Tian, ***Org. Electron.*** **38**, 8 (2016).
[36]D. Guo, Z. Andaji Garmaroudi, M. Abdi-Jalebi, S. D. Stranks and T. J. Savenije, ***ACS Energy Lett.*** **4** (10), 2360 (2019).
[37]R. Li, Y. Xu, W. Li, Y. Li, J. Peng, M. Xu and Q. Lin, ***J. Phys. Chem. Lett.*** **12** (6), 1726

(2021).
[38]M. Stolterfoht, B. Philippa, A. Armin, A. K. Pandey, R. D. White, P. L. Burn, P. Meredith and A. Pivrikas, ***Appl. Phys. Lett.*** **105** (1), 013302 (2014).
[39]B. Philippa, M. Stolterfoht, P. L. Burn, G. Juška, P. Meredith, R. D. White and A. Pivrikas, ***Sci. Rep.*** **4** (1), 5695 (2014).
[40]T. Kirchartz, W. Gong, S. A. Hawks, T. Agostinelli, R. C. I. Mackenzie, Y. Yang and J. Nelson, ***J. Phys. Chem. C*** **116** (14), 7672 (2012).
[41]D. V. Lang, ***J. Appl. Phys.*** **45** (7), 3023 (1974).
[42]Y. Xu, W. Li, T. Yu, Y. Li, R. Li and Q. Lin, ***Laser Photon. Rev.*** **15** (10), 2100169 (2021).